
Self-Supervised Policy Adaptation during Deployment

Nicklas Hansen
Technical University of Denmark

Yu Sun
UC Berkeley

Pieter Abbeel
UC Berkeley

Alexei A. Efros
UC Berkeley

Lerrel Pinto
UC Berkeley, NYU

Xiaolong Wang
UC Berkeley, UC San Diego

Abstract

In most real world scenarios, a policy trained by reinforcement learning in one environment needs to be deployed in another, potentially quite different environment. However, generalization across different environments is known to be hard. A natural solution would be to keep training after deployment in the new environment, but this cannot be done if the new environment offers no reward signal. Our work explores the use of self-supervision to allow the policy to continue training after deployment without using any rewards. While previous methods explicitly anticipate changes in the new environment, we assume no prior knowledge of those changes yet still obtain significant improvements. Empirical evaluations are performed on diverse environments from DeepMind Control suite and ViZDoom. Our method improves generalization in 25 out of 30 environments across various tasks, and outperforms domain randomization on a majority of environments.¹

1 Introduction

Deep reinforcement learning (RL) has achieved considerable success when combined with convolutional neural networks for deriving actions from image pixels [32, 27, 35, 68, 1]. However, one significant challenge for real-world deployment of vision-based RL remains: a policy trained in one environment might not generalize to other new environments not seen during training. Already hard for RL alone, the challenge is exacerbated when a policy faces high-dimensional visual inputs.

A well explored class of solutions is to learn robust policies that are simply invariant to changes in the environment [44, 60, 49, 43, 26]. For example, domain randomization [60, 40, 42, 69] applies data augmentation in a simulated environment to train a single robust policy, with the hope that the augmented environment covers enough factors of variation in the test environment. However, this hope may be difficult to realize when the test environment is truly unknown. With too much randomization, training a policy that can simultaneously fit numerous augmented environments requires much larger model and sample complexity. With too little randomization, the actual changes in the test environment might not be covered, and domain randomization may do more harm than good since the randomized factors are now irrelevant. Both phenomena have been observed in our experiments. In all cases, this class of solutions requires human experts to anticipate the changes before the test environment is seen. This cannot scale as more test environments are added with more diverse changes.

Instead of learning a robust policy *invariant* to all possible environmental changes, we argue that it is better for a policy to keep learning during deployment and *adapt* to its actual new environment. A naive way to implement this in RL is to fine-tune the policy in the new environment using rewards

¹Project page with code: <https://nicklashansen.github.io/PAD/>

as supervision [48]. However, while it is relatively easy to craft a dense reward function during training [13, 41], during deployment it is often impractical.

In this paper, we tackle an alternative problem setting in vision-based RL: adapting a pre-trained policy to an unknown environment without any reward. We do this by introducing self-supervision to obtain “free” training signal during deployment. Standard self-supervised learning employs auxiliary tasks designed to automatically create training labels using only the input data (see section 2 for details). Inspired by this, our policy is jointly trained with two objectives: a standard RL objective and, *additionally*, a self-supervised objective applied on an intermediate representation of the policy network. During training, both objectives are active, maximizing expected reward and simultaneously constraining the intermediate representation through self-supervision. During testing / deployment, only the self-supervised objective (on the raw observational data) remains active, forcing the intermediate representation to adapt to the new environment.

We experiment with two different self-supervised tasks, on two sets of environments: DeepMind Control suite [59] and the CRLMaze [29] ViZDoom [67] navigation task. We evaluate generalization by testing in new environments with changes unknown during training. Our method improves generalization in 19 out of 22 test environments across various tasks in DeepMind Control suite, and in 6 out of 8 test environments on CRLMaze, outperforming domain randomization on a majority of these environments.

2 Related Work

Self-supervised learning is a powerful way to learn visual representations from unlabeled data [62, 6, 63, 71, 38, 36, 72, 11]. Researchers have proposed to use auxiliary data prediction tasks, such as undoing rotation [11], solving a jigsaw puzzle [36], tracking [64], etc. to provide supervision in lieu of labels. In RL, the idea of learning visual representations and action at the same time has been investigated [23, 20, 39, 14, 70, 55, 24, 68]. For example, Srinivas et al. [55] use self-supervised contrastive learning techniques [4, 19, 66, 16] to improve sample efficiency in RL by jointly training the self-supervised objective and RL objective. However, this has not been shown to generalize to unseen environments. Other works have applied self-supervision for better generalization across environments [39, 7, 51]. For example, Pathak et al. [39] use a self-supervised prediction task to provide dense rewards for exploration in novel environments. While results on environment exploration from scratch are encouraging, how to transfer a trained policy (with extrinsic reward) to a novel environment remains unclear. Hence, these methods are not directly applicable to the proposed problem in our paper.

Generalization across different distributions is a central challenge in machine learning. In domain adaptation, target domain data is assumed to be accessible [9, 61, 8, 12, 30, 56]. For example, Tzeng et al. [61] use adversarial learning to align the feature representations in both the source and target domain during training. Similarly, the setting of domain generalization [10, 28, 31] assumes that all domains are sampled from the same meta distribution, but the same challenge remains and now becomes generalization across meta-distributions. Our work focuses instead on the setting of generalizing to truly *unseen* changes in the environment which cannot be anticipated at training time.

There have been several recent benchmarks in our setting for image recognition [17, 46, 47, 52]. For example, in Hendrycks and Dietterich [17], a classifier trained on regular images is tested on corrupted images, with corruption types unknown during training; the method of Hendrycks et al. [18] is proposed to improve robustness on this benchmark. Following similar spirit, in the context of RL, domain randomization [42, 60, 40, 45, 69] helps a policy trained in simulation to generalize to real robots. For example, Tobin et al. [60], Sadeghi and Levine [49] propose to render the simulation environment with random textures and train the policy on top. The learned policy is shown to generalize to real robot manipulation tasks. Instead of deploying a fixed policy, we train and adapt the policy to the new environment with observational data that is naturally revealed during deployment.

Test-time adaptation for deep learning is starting to be used in computer vision [53, 54, 3, 34, 57, 65]. For example, Shocher et al. [54] shows that image super-resolution can be learned at test time (from scratch) simply by trying to upsample a downsampled version of the input image. Bau et al. [3] show that adapting the prior of a generative adversarial network to the statistics of the test image improves photo manipulation tasks. Our work is closely related to the test-time training method of Sun et al. [57], which performs joint optimization of image recognition and self-supervised learning with rotation prediction [11], then uses the self-supervised objective to adapt the representation of each

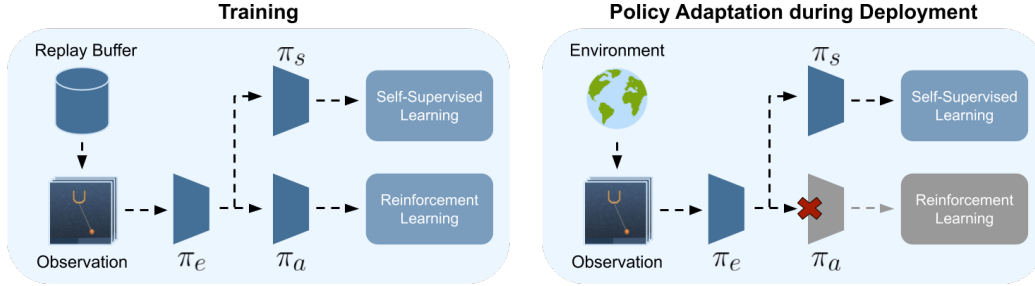


Figure 1. **Left:** training before deployment. For off-policy methods, observations are sampled from a replay buffer. For on-policy methods, observations are collected during roll-outs. We optimize both the RL and self-supervised objective. **Right:** Policy Adaptation during Deployment. Observations are collected from the test environment online with no memory, and we optimize only the self-supervised objective.

individual image during testing. Instead of image recognition, we perform test-time adaptation for RL with visual inputs in an online fashion. As the agent interacts with an environment using its policy, we can keep obtaining new observational data in a stream for training the visual representations.

3 Method

In this section, we describe our proposed Policy Adaptation during Deployment (PAD) approach. It can be implemented on top of any policy network and standard RL algorithm (both on-policy and off-policy) that can be described by minimizing some RL objective $J(\theta)$ w.r.t. the collection of parameters θ using stochastic gradient descent.

3.1 Network Architecture

We modify the network architecture to allow the policy and the self-supervised prediction to share features. For the collection of parameters θ of a given policy network π , we split it sequentially into $\theta = (\theta_e, \theta_a)$, where θ_e collects the parameters of the feature extractor, and θ_a is the head that outputs a distribution over actions. We define networks π_e with parameters θ_e and π_a with parameters θ_a such that $\pi(\mathbf{s}; \theta) = \pi_a(\pi_e(\mathbf{s}))$, where \mathbf{s} represents the input image observation. One can think of π_e as converting raw pixels to latent representations of physical quantities such as joint angles and locations, and π_a as a controller based on these quantities.

The goal of our method is to modify π_e at test time using gradients from a self-supervised task, such that π_e (and consequently π_θ) can generalize. Let π_s with parameters θ_s be the self-supervised prediction head and its collection of parameters, and the input to π_s be the output of π_e (refer to Figure 1 for an illustration of our method). In this work, the self-supervised task is inverse dynamics prediction for motor control, and rotation prediction for navigation.

3.2 Inverse Dynamics Prediction and Rotation Prediction

At each time step, we always observe a transition sequence in the form of $(\mathbf{s}_t, \mathbf{a}_t, \mathbf{s}_{t+1})$, during both training and testing. Naturally, self-supervision can be derived from taking parts of the sequence and predicting the rest. An inverse dynamics model takes the states before and after transition, and predicts the action in between. In this work, the inverse dynamics model π_s operates on the feature space extracted by π_e . We can write the inverse dynamics prediction objective formally as

$$L(\theta_s, \theta_e) = \ell(\mathbf{a}_t, \pi_s(\pi_e(\mathbf{s}_t), \pi_e(\mathbf{s}_{t+1}))) \quad (1)$$

For continuous actions, ℓ is the mean squared error between the ground truth and the model output. For discrete actions, the output is a soft-max distribution over the action space, and ℓ is the cross-entropy loss. Empirically, we find this self-supervised task to be most effective with continuous actions, possibly because inverse dynamics prediction in a small space of discrete actions is not as challenging. Note that we predict the inverse dynamics instead of the forward dynamics, because when operating on the feature space, the latter can produce trivial solutions such as the constant zero feature for every state. If we perform prediction with forward dynamics in pixel space, the task will be extremely challenging given the large uncertainty in pixel prediction.

As an alternative self-supervised task, we use the rotation prediction task [11]. We rotate an image by one of 0, 90, 180 and 270 degrees as input to the network, and cast this as a four-way classification problem to determine which one of these four ways the image has been rotated. This simple task is shown to be effective for learning representation for object configuration and scene structure, which is beneficial for diverse downstream visual recognition tasks [56, 18, 5].

3.3 Training and Testing

Before deployment of the policy, because we have signals from both the reward and self-supervised auxiliary task, we can train with both in the fashion of multi-task learning. This corresponds to the following optimization problem during training $\min_{\theta_a, \theta_s, \theta_e} J(\theta_a, \theta_e) + \alpha L(\theta_s, \theta_e)$, where $\alpha > 0$ is a trade-off hyper-parameter. During deployment, we cannot optimize J anymore since the reward is unavailable, but we can still optimize L to update both θ_s and θ_e . Empirically, we find only negligible difference with keeping θ_s fixed at test-time, so we simply update both since the gradients have to be calculated for both regardless. As we obtain new images from the stream of visual inputs in the environment, θ keeps being updated until the episode ends. This corresponds to, for each iteration $t = 1 \dots T$:

$$\mathbf{s}_t \sim p(\mathbf{s}_t | \mathbf{a}_{t-1}, \mathbf{s}_{t-1}) \tag{2}$$

$$\theta_s(t) = \theta_s(t-1) - \nabla_{\theta_s} L(x_t; \theta_s(t-1), \theta_e(t-1)) \tag{3}$$

$$\theta_e(t) = \theta_e(t-1) - \nabla_{\theta_e} L(x_t; \theta_s(t-1), \theta_e(t-1)) \tag{4}$$

$$\mathbf{a}_t = \pi(\mathbf{s}_t; \theta(t)) \quad \text{with} \quad \theta(t) = (\theta_e(t), \theta_a), \tag{5}$$

where $\theta_s(0) = \theta_s, \theta_e(0) = \theta_e, \mathbf{s}_0$ is the initial condition given by the environment, $\mathbf{a}_0 = \pi_{\theta}(\mathbf{s}_0)$, p is the unknown environment transition, and L is the self-supervised objective as previously introduced.

Our method above can also be interpreted from the perspective of adaptive control [2]. Equations (3) and (4) can be viewed as the internal dynamics of the controller, which performs parameter updates on the fly using feedback from the environment. It is widely recognized that while robust control is better for systems with abrupt changes, adaptive control is more suitable for systems with slow-varying deviations and uncertainties like seen in our paper [25, 50]. However, the main bottleneck for the widespread adoption of adaptive controllers is that designing suitable internal dynamics (update rules) for them is extremely hard from the control theory perspective and requires expert knowledge of the system. Instead, we opt for a generic self-supervised objective, and the internal dynamics are obtained through optimization on the objective rather than explicit design. That is, we automate the design of internal dynamics of an adaptive controller through learning.

4 Experiments

In this work, we investigate how well an agent trained in one environment (denoted as the *training environment*) generalizes to *unseen* test environments derived by making distinct environmental changes to the training environment. Specifically, we evaluate the episodic cumulative reward of our method (PAD) and baselines on continuous control tasks from DeepMind Control (DMC) suite [59] as well as the CRLMaze [29] navigation task, and experiment with both stationary (colors, objects, textures, lighting) and non-stationary (videos) environment changes. Agents have no access to any reward signal during deployment and is expected to generalize without pre-training or resetting within the test environment. As such, a good agent achieves a high cumulative reward in both training and test environments. Samples from the environments are shown in Figure 2. In this experimental setup, we further investigate how the choice of self-supervised task impacts our method and we show that PAD benefits tremendously from its online formulation. Our findings are detailed in the following.

4.1 DeepMind Control

DeepMind Control (DMC) [59] is a collection of continuous control tasks where agents only observe raw pixels. Generalization benchmarks on DMC represent diverse real-world tasks for motor control, and contain distracting surroundings that are not correlated with the reward signals.

Network details. Network architecture is adopted for all methods from Yarats et al. [70] but with certain modifications: the feature extractor π_e has 8 convolutional layers shared between the RL head π_a and self-supervised head π_s , and we split the network into architecturally identical heads

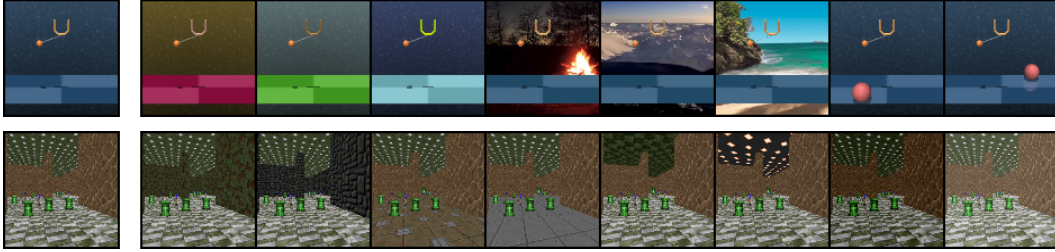


Figure 2. **Left:** Training environments of DMC (top) and CRLMaze (bottom). **Right:** Test environments of DMC (top) and CRLMaze (bottom). Changes to DMC include: randomized colors, video backgrounds, and distracting objects. The same environment changes are applied to all tasks in DMC. Changes to CRLMaze include the texture of walls, floor, and ceiling, as well as lighting.

Table 1. Cumulative reward in test environments with randomized colors, average of 10 seeds. Best method on each task is in bold and brown compares SAC+IDM with and without PAD.

Randomized colors	Blind	SAC	SAC (DR)	SAC+IDM	SAC+IDM (PAD)
Walker, walk	235 ± 17	414 ± 74	594 ± 104	406 ± 29	468 ± 47
Walker, stand	388 ± 10	719 ± 74	715 ± 96	743 ± 37	797 ± 46
Cartpole, swingup	132 ± 41	592 ± 50	647 ± 48	585 ± 73	630 ± 63
Cartpole, balance	646 ± 131	857 ± 60	867 ± 37	835 ± 40	848 ± 29
Ball in cup, catch	150 ± 96	411 ± 183	470 ± 252	471 ± 75	563 ± 50
Finger, spin	3 ± 2	626 ± 163	465 ± 314	757 ± 62	803 ± 72
Finger, turn_easy	172 ± 27	270 ± 43	167 ± 26	283 ± 51	304 ± 46
Cheetah, run	264 ± 75	154 ± 41	145 ± 29	121 ± 38	159 ± 28
Reacher, easy	107 ± 11	163 ± 45	105 ± 37	201 ± 32	214 ± 44

following π_e . Each head consists of 3 convolutional layers followed by 4 fully connected layers. Observations are stacks ($k = 3$) of colored frames, and random cropping is applied as in Srinivas et al. [55]. Hyper-parameters are taken directly from Yarats et al. [70]. During deployment, we optimize the self-supervised objective online w.r.t. θ_e, θ_s for one gradient step per time iteration. Implementation details are described further in appendix A.

Experimental setup. We experiment with 9 tasks from DMC and measure generalization to four types of test environments: (i) randomized colors of foreground, background and the agent itself; (ii) natural videos as background; (iii) distracting objects placed in the scene; and (iv) the unmodified training environment. For each test environment, we evaluate methods across 10 seeds and 100 randomly initialized episodes. When a given test environment is not applicable to a certain task, e.g. if the task has no background for the video background setting, it is excluded from the benchmark. Tasks are selected on the basis of diversity, as well as the success of vision-based RL in previous work [70, 55] on the tasks. On DMC, we apply our method to SAC [15] and use an inverse dynamics model (IDM) for self-supervision, as we find that learning a model of the motors works well for motor control. For completeness, we ablate the choice of self-supervision.

We compare our method to multiple baselines: (i) a blind agent without access to frames nor state, only observing its previous actions (denoted *Blind*); (ii) SAC with no modification (denoted *SAC*); (iii) SAC trained with domain randomization on a fixed set of 100 colors (denoted *SAC (DR)*); and finally (iv) SAC with an IDM but without PAD (denoted *SAC+IDM*). Our approach using SAC+IDM with PAD is denoted by *SAC+IDM (PAD)*. Colors in the randomized domain are sampled from the *same distribution* as evaluation, but with lower variance in pixel intensities, as we find that training directly on the test distribution is too hard and does not converge. We report results for all methods and highlight the best in bold, whereas brown color compares SAC+IDM with and without PAD.

Robustness to color change. Robustness to subtle changes such as color is essential to deployment of RL algorithms in the real world. We evaluate generalization of our method and baselines on a fixed set of 100 colors of foreground, background and the agent itself, and report the results in Table 1. We find that PAD improves generalization of SAC+IDM in all tasks considered, and outperforms SAC trained with domain randomization in 6 out of 9 tasks. Surprisingly, despite a significant overlap

Table 2. Cumulative reward in test environments with video backgrounds, average of 10 seeds. Best method on each task is in bold and brown compares SAC+IDM with and without PAD.

Video backgrounds	Blind	SAC	SAC (DR)	SAC+IDM	SAC+IDM (PAD)
Walker, walk	235 ± 17	616 ± 80	655 ± 55	694 ± 85	717 ± 79
Walker, stand	388 ± 10	899 ± 53	869 ± 60	902 ± 51	935 ± 20
Cartpole, swingup	132 ± 41	375 ± 90	485 ± 67	487 ± 90	521 ± 76
Cartpole, balance	646 ± 131	693 ± 109	766 ± 92	691 ± 76	687 ± 58
Ball in cup, catch	150 ± 96	393 ± 175	271 ± 189	362 ± 69	436 ± 55
Finger, spin	3 ± 2	447 ± 102	338 ± 207	605 ± 61	691 ± 80
Finger, turn_easy	172 ± 27	355 ± 108	223 ± 91	355 ± 110	362 ± 101
Cheetah, run	264 ± 75	194 ± 30	150 ± 34	164 ± 42	206 ± 34

Table 3. Cumulative reward in test environments with distracting objects, average of 10 seeds. Best method on each task is in bold and brown compares SAC+IDM with and without PAD.

Distracting objects	Blind	SAC	SAC (DR)	SAC+IDM	SAC+IDM (PAD)
Cartpole, swingup	132 ± 41	815 ± 60	809 ± 24	776 ± 58	771 ± 64
Cartpole, balance	646 ± 131	969 ± 20	938 ± 35	964 ± 26	960 ± 29
Ball in cup, catch	150 ± 96	177 ± 111	331 ± 189	482 ± 128	545 ± 173
Finger, spin	3 ± 2	652 ± 184	564 ± 288	836 ± 62	867 ± 72
Finger, turn_easy	172 ± 27	302 ± 68	165 ± 12	326 ± 101	347 ± 48

between the test domain and its training domain, domain randomization generalizes no better than vanilla SAC on a majority of the tasks. Further, we find that the relative improvement of PAD improves over time, as shown in Figure 3, and our method thus naturally extends beyond episodic deployment.

Non-stationary test environments. In the previous experiment, we show that our method can adapt to stationary changes in the test environment. In real-world deployments, however, environments are rarely static. To explore whether PAD can adapt to non-stationary environments, we evaluate generalization to 10 video backgrounds (refer to Figure 2). As shown in Table 2, our method outperforms all baselines in 6 out of 8 tasks, often by a large margin. Domain randomization generalizes comparably worse to videos, which we conjecture is not because test environments are non-stationary, but rather because the image statistics of videos are not covered by the randomized color distribution that it was trained on. In fact, domain randomization is outperformed by the vanilla SAC algorithm in a majority of tasks with video backgrounds, which is in line with the findings of Packer et al. [37].

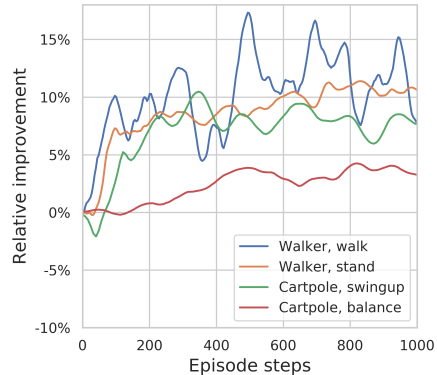


Figure 3. Relative improvement in instantaneous reward over time for our method on the 100-color environment in DMC. We show here three tasks in which PAD improves by a large margin and one task where it does not.

Generalization in scene contents. Orthogonal to changes in color and background, scene contents themselves can be considered a change of environment. We hypothesize that: (i) an agent trained with an IDM is comparably less distracted by scene content unrelated to the task at hand; and (ii) that PAD can adapt to unexpected objects in the scene. We test these hypotheses by placing an alien object (a red ball) in the scene and observe robustness to a total of 28 different object positions in both the foreground and background of the scene. There is no physical interaction between the placed objects and the agent. Empirical results are shown in Table 3. We find that our method improves SAC+IDM and outperforms all other baselines in 3 out of 5 tasks, and by a large margin in two of those tasks. All methods are relatively unaffected by objects in the two cartpole tasks.

Training and testing in the same environment. In simulation, agents are typically trained and tested on the same environment. For completeness, we also evaluate our method in this setting

Table 4. Cumulative reward of our method and baselines on the training environment for each of the 9 tasks considered in DMC, average of 10 seeds. Best method on each task is in bold and brown compares SAC+IDM with and without PAD. PAD hurts minimally when environment is unchanged.

Training env.	Blind	SAC	SAC (DR)	SAC+IDM	SAC+IDM (PAD)
Walker, walk	235 ± 17	847 ± 71	756 ± 71	911 ± 24	895 ± 28
Walker, stand	388 ± 10	959 ± 11	928 ± 36	966 ± 8	956 ± 20
Cartpole, swingup	132 ± 41	850 ± 28	807 ± 36	849 ± 30	845 ± 34
Cartpole, balance	646 ± 131	978 ± 22	971 ± 30	982 ± 20	979 ± 21
Ball in cup, catch	150 ± 96	725 ± 355	469 ± 339	919 ± 118	910 ± 129
Finger, spin	3 ± 2	809 ± 138	686 ± 295	928 ± 45	927 ± 45
Finger, turn_easy	172 ± 27	462 ± 146	243 ± 124	462 ± 152	455 ± 160
Cheetah, run	264 ± 75	387 ± 74	195 ± 46	384 ± 88	380 ± 91
Reacher, easy	107 ± 11	264 ± 113	92 ± 45	390 ± 126	365 ± 114

Table 5. Ablations on the randomized color test domain of DMC. All methods implicitly use SAC. CURL represents RL with a contrastive learning task [55] and Rot represents rotation prediction task [11]. Offline PAD is here denoted O-PAD for brevity, whereas the default usage of PAD is in an online setting. Best method is in bold and brown compares SAC+IDM with and without PAD.

Randomized colors	CURL	CURL (PAD)	Rot	Rot (PAD)	IDM	IDM (O-PAD)	IDM (PAD)
Walker, walk	445 ± 99	495 ± 70	335 ± 7	330 ± 30	406 ± 29	441 ± 16	468 ± 47
Walker, stand	662 ± 54	753 ± 49	673 ± 4	653 ± 27	743 ± 37	727 ± 21	797 ± 46
Cartpole, swingup	454 ± 110	413 ± 67	493 ± 52	477 ± 38	585 ± 73	578 ± 69	630 ± 63
Cartpole, balance	782 ± 13	763 ± 5	710 ± 72	734 ± 81	835 ± 40	796 ± 37	848 ± 29
Ball in cup, catch	231 ± 92	332 ± 78	291 ± 54	314 ± 60	471 ± 75	490 ± 16	563 ± 50
Finger, spin	691 ± 12	588 ± 22	695 ± 36	689 ± 20	757 ± 62	767 ± 43	803 ± 72
Finger, turn_easy	202 ± 32	186 ± 2	283 ± 68	230 ± 53	283 ± 51	321 ± 10	304 ± 46
Cheetah, run	202 ± 22	211 ± 20	127 ± 3	135 ± 12	121 ± 38	112 ± 35	159 ± 28
Reacher, easy	325 ± 32	378 ± 62	99 ± 29	120 ± 7	201 ± 32	241 ± 24	214 ± 44

and results are shown in Table 4. We show that, while PAD improves generalization to novel test environments, the performance of SAC+IDM is virtually unchanged by PAD on the training environment but still outperforms baselines on most tasks, which we hypothesize is because the self-supervised objective improves learning by constraining the intermediate representation of policies.

Choice of self-supervised task. We examine how much the choice of self-supervised task contributes to the overall success of our method, and consider the following ablations: (i) replacing inverse dynamics with the rotation prediction task described in subsection 3.2; and (ii) replacing it with the recently proposed CURL [55] contrastive learning algorithm for RL. As shown in Table 5, PAD improves generalization of CURL in a majority of tasks on the randomized color benchmark, and in 4 out of 9 tasks using rotation prediction. However, inverse dynamics as auxiliary task produces more consistent results and offers better generalization overall. We argue that learning inverse dynamics produces better representations for motor control since it connects observations directly to actions, whereas CURL and rotation prediction operates purely on observations.

Offline versus online learning. Since observations that arrive sequentially usually are highly correlated, we hypothesize that our method benefits significantly from learning online. To test this hypothesis, we run an *offline* variant of our method in which network updates are "forgotten" after each step. In this setting, our method can only adapt to single observations and do not benefit from learning over time. Results are shown in Table 5. We find that our method benefits tremendously from online learning, but learning offline still improves generalization on a number of tasks.

4.2 CRLMaze

CRLMaze [29] is a time-constrained navigation task for ViZDoom [67], in which an agent is to navigate around a maze and collect objects. An agent has valid actions $\mathcal{A} = \{\text{MoveForward}, \text{TurnLeft}, \text{TurnRight}\}$. There is a positive reward associated with green columns and a negative reward for picking up lanterns, as well as a small negative reward for living. Readers are referred to the respective papers for details on the environment.

Table 6. Cumulative reward on the training environment and eight novel environments for CRLMaze, averaged over 10 seeds. Best method is in bold and brown compares A2C+Rot (rotation prediction) with and without PAD. Our method improves generalization on a majority of environments.

CRLMaze	Random	A2C	A2C (DR)	A2C+IDM	A2C+IDM (PAD)	A2C+Rot	A2C+Rot (PAD)
Training env.	-868 ± 108	371 ± 629	-355 ± 295	585 ± 781	-416 ± 428	729 ± 471	681 ± 316
Walls (1)	-877 ± 136	-6 ± 571	-355 ± 260	157 ± 738	-475 ± 356	124 ± 586	204 ± 285
Walls (2)	-864 ± 60	-754 ± 351	-166 ± 609	-761 ± 214	-381 ± 502	-536 ± 468	-353 ± 453
Floor (1)	-872 ± 69	-93 ± 599	-435 ± 193	156 ± 725	-537 ± 321	-79 ± 562	114 ± 369
Floor (2)	-864 ± 80	-548 ± 460	-441 ± 186	-251 ± 530	-524 ± 355	-509 ± 412	-533 ± 232
Ceiling (1)	-909 ± 93	-84 ± 567	-388 ± 248	264 ± 736	-543 ± 289	326 ± 394	316 ± 278
Ceiling (2)	-836 ± 100	-259 ± 542	-412 ± 225	68 ± 632	-474 ± 372	-69 ± 459	247 ± 252
Light (1)	-893 ± 78	-382 ± 740	-332 ± 348	-134 ± 820	-525 ± 383	-538 ± 375	171 ± 293
Light (2)	-908 ± 109	321 ± 612	-288 ± 328	612 ± 889	-396 ± 339	369 ± 712	453 ± 368

Network details. The neural networks implementing π_e , π_a , and π_s for CRLMaze are architecturally similar to that of DMC, but with two subtle differences: π_e only consists of 6 convolutional layers, and task heads π_a , π_s each have three fully connected layers. Like for DMC, observations are frame stacks ($k = 3$) of dimensions 100x100 and we crop to 84x84. We adopt hyperparameters from Lomonaco et al. [29] and jointly optimize both the RL objective and self-supervised objective during training. At test-time, we use the sequentially arriving observations to optimize the self-supervised objective, making one gradient update to network parameters θ_e , θ_s at each environment step. Implementation details are described further in appendix A.

Experimental setup. We train agents on a single environment and measure generalization on a total of eight novel test environments. Each environment contains a single modification to the training environment in the form of textures for walls, floor and ceiling, as well as lighting, as shown in Figure 2. We apply PAD to A2C, a synchronous variant of A3C [33], and use rotation prediction (see subsection 3.2) as the self-supervised task. Navigation tasks require scene understanding, and we find that rotation prediction facilitates learning such representations more so than an learning Inverse Dynamics Model.

We compare to the following baselines: (i) a random agent sampling actions from a uniform distribution (denoted *Random*); (ii) A2C with no modifications (denoted *A2C*); (iii) A2C trained with domain randomization (denoted *A2C (DR)*); and (iv) A2C with rotation prediction as auxiliary task (denoted *A2C+Rot*; without PAD). We denote A2C+Rot with PAD as *A2C+Rot (PAD)*. The randomized domain consists of 56 combinations of diverse textures for walls, floor and ceiling, including textures from the training environment of other methods, such that there is an overlap between training and test distributions. In each test environment, we evaluate methods on 20 starting positions and report results across 10 seeds for all methods. In the reported results, bold denotes best method whereas brown color is a comparison of A2C+Rot with and without PAD.

Generalization in navigation tasks. Learning to navigate in novel scenes is a challenging problem because it requires a generalized scene understanding. We hypothesize that: (i) rotation prediction learns representations that are useful for scene understanding; and (ii) PAD can adapt those representations to novel scenes. Results from experiments are shown in Table 6. PAD improves generalization of A2C+Rot in 5 out of 8 test environments considered, and outperforms domain randomization on both the training environment and a total of 6 test environments. Further, we emphasize that rotation prediction itself also improves in-domain performance as well as generalization compared to a vanilla A2C, and that PAD decreases variance between seeds by a large margin.

Choice of self-supervised task. While an auxiliary task can enforce structure in the learned representations, its gradients need to be sufficiently correlated with the primary RL task for PAD to be successful. We examine the importance of selecting appropriate auxiliary tasks by a simple ablation: replacing rotation prediction with an IDM for the navigation task (denoted *A2C+IDM*). As can be seen in Table 6, PAD with IDM (denoted *A2C+IDM (PAD)*) hurts performance in all environments considered, while rotation prediction generally improves performance. We argue that navigation tasks require scene understanding and that rotation prediction promotes that more so than an inverse dynamics model.

5 Conclusion

While previous work addresses generalization in RL by learning policies that are invariant to any environment changes that can be anticipated, we formulate an alternative problem setting in vision-based RL: can we instead *adapt* a pretrained-policy to new environments without any reward. We propose Policy Adaptation during Deployment, a self-supervised framework for online adaptation at test-time, and show empirically that our method improves generalization of policies to diverse simulated environmental changes across a variety of tasks. We find that Policy Adaptation during Deployment benefits greatly from learning online, and we systematically evaluate how the choice of self-supervised task impacts performance. While the current framework still relies on prior knowledge on selecting self-supervised tasks for policy adaptation, we see our work as the initial step in addressing the problem of adapting vision-based policies to unknown environments. We ultimately envision embodied agents in the future to be learning all the time, with the flexibility to learn both with and without reward signals, before and during deployment.

Acknowledgements. This work is supported by NSF grant IIS 1633310, DARPA LwLL project, grants from SAP and Berkeley DeepDrive. The authors would like to thank Fenglu Hong and Joey Hejna for helpful discussions.

References

- [1] O. M. Andrychowicz, B. Baker, M. Chociej, R. Jozefowicz, B. McGrew, J. Pachocki, A. Petron, M. Plappert, G. Powell, A. Ray, et al. Learning dexterous in-hand manipulation. *The International Journal of Robotics Research*, 39(1):3–20, 2020.
- [2] K. J. Åström and B. Wittenmark. *Adaptive control*. Courier Corporation, 2013.
- [3] D. Bau, H. Strobel, W. Peebles, J. Wulff, B. Zhou, J.-Y. Zhu, and A. Torralba. Semantic photo manipulation with a generative image prior. *ACM Trans. Graph.*, 38(4), 2019. ISSN 0730-0301.
- [4] T. Chen, S. Kornblith, M. Norouzi, and G. Hinton. A simple framework for contrastive learning of visual representations, 2020.
- [5] C. Doersch and A. Zisserman. Multi-task self-supervised visual learning. In *Proceedings of the IEEE International Conference on Computer Vision*, pages 2051–2060, 2017.
- [6] C. Doersch, A. Gupta, and A. A. Efros. Unsupervised visual representation learning by context prediction. In *Proceedings of the IEEE International Conference on Computer Vision*, pages 1422–1430, 2015.
- [7] F. Ebert, C. Finn, S. Dasari, A. Xie, A. Lee, and S. Levine. Visual foresight: Model-based deep reinforcement learning for vision-based robotic control, 2018.
- [8] Y. Ganin, E. Ustinova, H. Ajakan, P. Germain, H. Larochelle, F. Laviolette, M. Marchand, and V. Lempitsky. Domain-adversarial training of neural networks. *The Journal of Machine Learning Research*, 17(1):2096–2030, 2016.
- [9] R. Geirhos, C. R. M. Temme, J. Rauber, H. H. Schütt, M. Bethge, and F. A. Wichmann. Generalisation in humans and deep neural networks. In *NeurIPS*, 2018.
- [10] M. Ghifary, W. B. Kleijn, M. Zhang, and D. Balduzzi. Domain generalization for object recognition with multi-task autoencoders. In *Proceedings of the 2015 IEEE International Conference on Computer Vision (ICCV), ICCV '15*, page 2551–2559. IEEE Computer Society, 2015. ISBN 9781467383912.
- [11] S. Gidaris, P. Singh, and N. Komodakis. Unsupervised representation learning by predicting image rotations, 2018.
- [12] B. Gong, Y. Shi, F. Sha, and K. Grauman. Geodesic flow kernel for unsupervised domain adaptation. In *2012 IEEE Conference on Computer Vision and Pattern Recognition*, pages 2066–2073. IEEE, 2012.

- [13] S. Gu, E. Holly, T. Lillicrap, and S. Levine. Deep reinforcement learning for robotic manipulation with asynchronous off-policy updates. In *2017 IEEE international conference on robotics and automation (ICRA)*, pages 3389–3396. IEEE, 2017.
- [14] D. Ha and J. Schmidhuber. Recurrent world models facilitate policy evolution. In *Advances in Neural Information Processing Systems 31*, pages 2451–2463. Curran Associates, Inc., 2018.
- [15] T. Haarnoja, A. Zhou, K. Hartikainen, G. Tucker, S. Ha, J. Tan, V. Kumar, H. Zhu, A. Gupta, P. Abbeel, and S. Levine. Soft actor-critic algorithms and applications, 2018.
- [16] K. He, H. Fan, Y. Wu, S. Xie, and R. Girshick. Momentum contrast for unsupervised visual representation learning. In *Proceedings of the IEEE Conference on Computer Vision and Pattern Recognition*, 2020.
- [17] D. Hendrycks and T. G. Dietterich. Benchmarking neural network robustness to common corruptions and surface variations. *arXiv: Learning*, 2018.
- [18] D. Hendrycks, M. Mazeika, S. Kadavath, and D. Song. Using self-supervised learning can improve model robustness and uncertainty. *ArXiv*, abs/1906.12340, 2019.
- [19] O. J. Hénaff, A. Srinivas, J. D. Fauw, A. Razavi, C. Doersch, S. M. A. Eslami, and A. van den Oord. Data-efficient image recognition with contrastive predictive coding, 2019.
- [20] M. Jaderberg, V. Mnih, W. M. Czarnecki, T. Schaul, J. Z. Leibo, D. Silver, and K. Kavukcuoglu. Reinforcement learning with unsupervised auxiliary tasks, 2016.
- [21] I. Kostrikov, D. Yarats, and R. Fergus. Image augmentation is all you need: Regularizing deep reinforcement learning from pixels. 2020.
- [22] A. Krizhevsky, I. Sutskever, and G. E. Hinton. Imagenet classification with deep convolutional neural networks. In *NIPS*, 2012.
- [23] S. Lange and M. A. Riedmiller. Deep auto-encoder neural networks in reinforcement learning. In *The 2010 International Joint Conference on Neural Networks (IJCNN)*, pages 1–8, 2010.
- [24] M. Laskin, K. Lee, A. Stooke, L. Pinto, P. Abbeel, and A. Srinivas. Reinforcement learning with augmented data. *arXiv preprint arXiv:2004.14990*, 2020.
- [25] E. Lavretsky. Adaptive control: Introduction, overview, and applications. In *Lecture notes from IEEE Robust and Adaptive Control Workshop*, 2008.
- [26] K. Lee, K. Lee, J. Shin, and H. Lee. A simple randomization technique for generalization in deep reinforcement learning. *ArXiv*, abs/1910.05396, 2019.
- [27] S. Levine, C. Finn, T. Darrell, and P. Abbeel. End-to-end training of deep visuomotor policies. *The Journal of Machine Learning Research*, 17(1):1334–1373, 2016.
- [28] Y. F. Li, M. Gong, X. Tian, T. Liu, and D. Tao. Domain generalization via conditional invariant representations. In *AAAI*, 2018.
- [29] V. Lomonaco, K. Desai, E. Culurciello, and D. Maltoni. Continual reinforcement learning in 3d non-stationary environments. *arXiv preprint arXiv:1905.10112*, 2019.
- [30] M. Long, H. Zhu, J. Wang, and M. I. Jordan. Unsupervised domain adaptation with residual transfer networks. In *Advances in Neural Information Processing Systems*, pages 136–144, 2016.
- [31] T. Matsuura and T. Harada. Domain generalization using a mixture of multiple latent domains, 2019.
- [32] V. Mnih, K. Kavukcuoglu, D. Silver, A. Graves, I. Antonoglou, D. Wierstra, and M. Riedmiller. Playing atari with deep reinforcement learning. *arXiv preprint arXiv:1312.5602*, 2013.
- [33] V. Mnih, A. P. Badia, M. Mirza, A. Graves, T. P. Lillicrap, T. Harley, D. Silver, and K. Kavukcuoglu. Asynchronous methods for deep reinforcement learning, 2016.

- [34] R. T. Mullapudi, S. Chen, K. Zhang, D. Ramanan, and K. Fatahalian. Online model distillation for efficient video inference. *2019 IEEE/CVF International Conference on Computer Vision (ICCV)*, Oct 2019. doi: 10.1109/iccv.2019.00367.
- [35] A. V. Nair, V. Pong, M. Dalal, S. Bahl, S. Lin, and S. Levine. Visual reinforcement learning with imagined goals. In *Advances in Neural Information Processing Systems*, pages 9191–9200, 2018.
- [36] M. Noroozi and P. Favaro. Unsupervised learning of visual representations by solving jigsaw puzzles. In *European Conference on Computer Vision*, pages 69–84. Springer, 2016.
- [37] C. Packer, K. Gao, J. Kos, P. Krähenbühl, V. Koltun, and D. Song. Assessing generalization in deep reinforcement learning, 2018.
- [38] D. Pathak, P. Krahenbuhl, J. Donahue, T. Darrell, and A. A. Efros. Context encoders: Feature learning by inpainting. In *Proceedings of the IEEE conference on computer vision and pattern recognition*, pages 2536–2544, 2016.
- [39] D. Pathak, P. Agrawal, A. A. Efros, and T. Darrell. Curiosity-driven exploration by self-supervised prediction. In *ICML*, 2017.
- [40] X. B. Peng, M. Andrychowicz, W. Zaremba, and P. Abbeel. Sim-to-real transfer of robotic control with dynamics randomization. *2018 IEEE International Conference on Robotics and Automation (ICRA)*, May 2018.
- [41] L. Pinto and A. Gupta. Supersizing self-supervision: Learning to grasp from 50k tries and 700 robot hours. In *2016 IEEE international conference on robotics and automation (ICRA)*, pages 3406–3413. IEEE, 2016.
- [42] L. Pinto, M. Andrychowicz, P. Welinder, W. Zaremba, and P. Abbeel. Asymmetric actor critic for image-based robot learning. *arXiv preprint arXiv:1710.06542*, 2017.
- [43] L. Pinto, J. Davidson, R. Sukthankar, and A. Gupta. Robust adversarial reinforcement learning. In *Proceedings of the 34th International Conference on Machine Learning-Volume 70*, pages 2817–2826. JMLR. org, 2017.
- [44] A. Rajeswaran, S. Ghotra, B. Ravindran, and S. Levine. Epopt: Learning robust neural network policies using model ensembles. *arXiv preprint arXiv:1610.01283*, 2016.
- [45] F. Ramos, R. Possas, and D. Fox. Bayessim: Adaptive domain randomization via probabilistic inference for robotics simulators. *Robotics: Science and Systems XV*, Jun 2019.
- [46] B. Recht, R. Roelofs, L. Schmidt, and V. Shankar. Do cifar-10 classifiers generalize to cifar-10? *arXiv preprint arXiv:1806.00451*, 2018.
- [47] B. Recht, R. Roelofs, L. Schmidt, and V. Shankar. Do imagenet classifiers generalize to imagenet? *arXiv preprint arXiv:1902.10811*, 2019.
- [48] A. A. Rusu, N. C. Rabinowitz, G. Desjardins, H. Soyer, J. Kirkpatrick, K. Kavukcuoglu, R. Pascanu, and R. Hadsell. Progressive neural networks. *arXiv preprint arXiv:1606.04671*, 2016.
- [49] F. Sadeghi and S. Levine. Cad2rl: Real single-image flight without a single real image. *arXiv preprint arXiv:1611.04201*, 2016.
- [50] S. Sastry and M. Bodson. *Adaptive control: stability, convergence and robustness*. Courier Corporation, 2011.
- [51] R. Sekar, O. Rybkin, K. Daniilidis, P. Abbeel, D. Hafner, and D. Pathak. Planning to explore via self-supervised world models, 2020.
- [52] V. Shankar, A. Dave, R. Roelofs, D. Ramanan, B. Recht, and L. Schmidt. A systematic framework for natural perturbations from videos. *arXiv preprint arXiv:1906.02168*, 2019.

- [53] A. Shocher, N. Cohen, and M. Irani. Zero-shot super-resolution using deep internal learning, 2017.
- [54] A. Shocher, S. Bagon, P. Isola, and M. Irani. Ingan: Capturing and remapping the "dna" of a natural image, 2018.
- [55] A. Srinivas, M. Laskin, and P. Abbeel. Curl: Contrastive unsupervised representations for reinforcement learning. *arXiv preprint arXiv:2004.04136*, 2020.
- [56] Y. Sun, E. Tzeng, T. Darrell, and A. A. Efros. Unsupervised domain adaptation through self-supervision. *arXiv preprint*, 2019.
- [57] Y. Sun, X. Wang, Z. Liu, J. Miller, A. A. Efros, and M. Hardt. Test-time training with self-supervision for generalization under distribution shifts. *ICML*, 2020.
- [58] C. Szegedy, W. Liu, Y. Jia, P. Sermanet, S. Reed, D. Anguelov, D. Erhan, V. Vanhoucke, and A. Rabinovich. Going deeper with convolutions. *2015 IEEE Conference on Computer Vision and Pattern Recognition (CVPR)*, pages 1–9, 2015.
- [59] Y. Tassa, Y. Doron, A. Muldal, T. Erez, Y. Li, D. de Las Casas, D. Budden, A. Abdolmaleki, J. Merel, A. Lefrancq, T. Lillicrap, and M. Riedmiller. DeepMind control suite. Technical report, DeepMind, Jan. 2018.
- [60] J. Tobin, R. Fong, A. Ray, J. Schneider, W. Zaremba, and P. Abbeel. Domain randomization for transferring deep neural networks from simulation to the real world. *2017 IEEE/RSJ International Conference on Intelligent Robots and Systems (IROS)*, Sep 2017.
- [61] E. Tzeng, J. Hoffman, K. Saenko, and T. Darrell. Adversarial discriminative domain adaptation. In *Proceedings of the IEEE Conference on Computer Vision and Pattern Recognition*, pages 7167–7176, 2017.
- [62] P. Vincent, H. Larochelle, Y. Bengio, and P.-A. Manzagol. Extracting and composing robust features with denoising autoencoders. In *Proceedings of the 25th international conference on Machine learning*, pages 1096–1103. ACM, 2008.
- [63] X. Wang and A. Gupta. Unsupervised learning of visual representations using videos. In *ICCV*, 2015.
- [64] X. Wang, A. Jabri, and A. A. Efros. Learning correspondence from the cycle-consistency of time. In *CVPR*, 2019.
- [65] M. Wortsman, K. Ehsani, M. Rastegari, A. Farhadi, and R. Mottaghi. Learning to learn how to learn: Self-adaptive visual navigation using meta-learning, 2018.
- [66] Z. Wu, Y. Xiong, S. X. Yu, and D. Lin. Unsupervised feature learning via non-parametric instance discrimination. In *Proceedings of the IEEE Conference on Computer Vision and Pattern Recognition*, pages 3733–3742, 2018.
- [67] M. Wydmuch, M. Kempka, and W. Jaśkowski. Vizdoom competitions: Playing doom from pixels. *IEEE Transactions on Games*, 2018.
- [68] W. Yan, A. Vangipuram, P. Abbeel, and L. Pinto. Learning predictive representations for deformable objects using contrastive estimation. *arXiv preprint arXiv:2003.05436*, 2020.
- [69] J. Yang, B. Petersen, H. Zha, and D. Faissol. Single episode policy transfer in reinforcement learning, 2019.
- [70] D. Yarats, A. Zhang, I. Kostrikov, B. Amos, J. Pineau, and R. Fergus. Improving sample efficiency in model-free reinforcement learning from images, 2019.
- [71] R. Zhang, P. Isola, and A. A. Efros. Colorful image colorization. In *European conference on computer vision*, pages 649–666. Springer, 2016.
- [72] R. Zhang, P. Isola, and A. A. Efros. Split-brain autoencoders: Unsupervised learning by cross-channel prediction. In *Proceedings of the IEEE Conference on Computer Vision and Pattern Recognition*, pages 1058–1067, 2017.

Table 7. Hyper-parameters for the DMC tasks.

Hyperparameter	Value
Frame rendering	$3 \times 100 \times 100$
Frame after crop	$3 \times 84 \times 84$
Stacked frames	3
Action repeat	2 (finger) 8 (cartpole) 4 (otherwise)
Discount factor γ	0.99
Episode length	1,000
Learning algorithm	Soft Actor-Critic
Self-supervised task	Inverse Dynamics Model
Number of training steps	500,000
Replay buffer size	500,000
Optimizer (π^e, π^a, π^s)	Adam ($\beta_1 = 0.9, \beta_2 = 0.999$)
Optimizer (α)	Adam ($\beta_1 = 0.5, \beta_2 = 0.999$)
Learning rate (π^e, π^a, π^s)	$3e-4$ (cheetah) $1e-3$ (otherwise)
Learning rate (α)	$1e-4$
Batch size	128
Batch size (test-time)	32
π^e, π^s update freq.	2
π^e, π^s update freq. (test-time)	1

Table 8. Hyper-parameters for the CRLMaze task.

Hyperparameter	Value
Frame rendering	$3 \times 100 \times 100$
Frame after crop	$3 \times 84 \times 84$
Stacked frames	3
Action repeat	4
Discount factor γ	0.99
Episode length	1,000
Learning algorithm	Advantage Actor-Critic
Self-supervised task	Rotation Prediction
Number of training episodes	1,000 (dom. rand.) 500 (otherwise)
Number of processes	20
Optimizer	Adam ($\beta_1 = 0.9, \beta_2 = 0.999$)
Learning rate	$1e-4$
Learning rate (test-time)	$1e-5$
Batch size	20
Batch size (test-time)	32
π^e, π^s loss coefficient	0.5
π^e, π^s loss coefficient (test-time)	1
π^e, π^s update freq.	1
π^e, π^s update freq. (test-time)	1

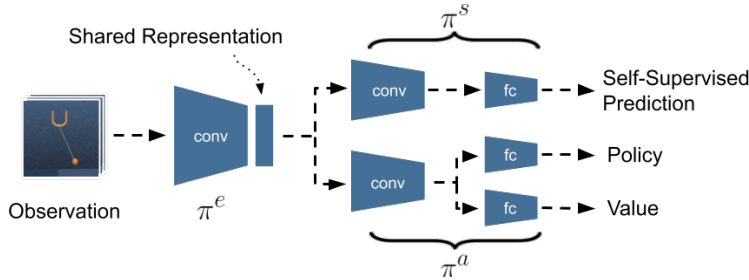


Figure 4. Network architecture for the DMC and CRLMaze experiments. π^s and π^a uses a shared feature extractor π^e . Implementation of policy and value function depends on the learning algorithm.

A Implementation Details

In this section, we elaborate on implementation details for our experiments on DeepMind Control (DMC) suite [59] and CRLMaze [29] for ViZDoom [67].

Architecture. Our network architecture is illustrated in Figure 4. Observations are stacked frames ($k = 3$) rendered at 100×100 and cropped to 84×84 , i.e. inputs to the network are of dimensions $9 \times 84 \times 84$, where the first dimension indicates the channel numbers and the following ones represent spatial dimensions. The same crop is applied to all frames in a stack. The shared feature extractor π^e consists of 8 (DMC) or 6 (CRLMaze) convolutional layers and outputs features of size $32 \times 21 \times 21$ in DMC and size $32 \times 25 \times 25$ in CRLMaze. The output from π^e is used as input to both the self-supervised head π^s and RL head π^a , both of which consist of 3 convolutional layers followed by 3 fully-connected layers.

Learning algorithm. We use Soft Actor-Critic (SAC) [15] for DMC and Advantage Actor-Critic (A2C) for CRLMaze. Network outputs depend on the task and learning algorithm. As the action space of DMC is continuous, the policy learned by SAC outputs the mean and variance of a Gaussian distribution over actions. CRLMaze has a discrete action space and the policy learned by A2C thus learns a soft-max distribution over actions. For details on the critics learned by SAC and A2C, the reader is referred to Haarnoja et al. [15] and Mnih et al. [33], respectively.

Hyper-parameters. When applicable, we adopt our hyper-parameters from Yarats et al. [70] (DMC) and Lomonaco et al. [29] (CRLMaze). For completeness, we detail all hyper-parameters used for the two environments in Table 7 and Table 8.

Data augmentation. Random cropping is a commonly used data augmentation used in computer vision systems [22, 58] but has only recently gained interest as a stochastic regularization technique in the RL literature [55, 21, 24]. We adopt the random crop proposed in Srinivas et al. [55]: crop rendered observations of size 100×100 to 84×84 , applying the same crop to all frames in a stacked observation. This has the added benefits of regularization while still preserving spatio-temporal patterns between frames. When learning an Inverse Dynamics Model, we apply the same crop to all frames of a given observation but apply two different crops to the consecutive observations $(\mathbf{s}_t, \mathbf{s}_{t+1})$ used to predict action \mathbf{a}_t .

Policy Adaptation during Deployment. We evaluate our method and baselines with episodic cumulative reward of an agent trained in a single environment and tested in a collection of test environments, each with distinct changes from the training environment. We assume no reward signal at test-time and agents are expected to generalize without pre-training or resetting in the new environment. Therefore, we make updates to the policy using a self-supervised objective, and we train using observations from the environment in an online manner without memory, i.e. we make one update per step using the most-recent observation.

Empirically, we find that: (i) the random crop data augmentation used during training helps regularize learning at test-time; and (ii) our algorithm benefits from learning from a batch of randomly cropped observations rather than single observations, even when all observations in the batch are augmented copies of the most-recent observation. As such, we apply both of these techniques when performing Policy Adaptation during Deployment and use a batch size of 32. When using the policy to take actions, however, inputs to the policy are simply center-cropped.